European Journal of Mechanics / A Solids 96 (2022) 104661

Contents lists available at ScienceDirect

European Journal of Mechanics / A Solids

journal homepage: www.elsevier.com/locate/ejmsol

# Experimental and numerical investigations of the electro-mechanical response of particle filled elastomers—Part II: Continuum modeling approach

Markus Mehnert [a,*], Jessica Faber [a], Mokarram Hossain [b], Shawn A. Chester [c], Paul Steinmann [a,d]

[a] Institute of Applied Mechanics, University of Erlangen–Nuremberg, Egerlandstr. 5, 91058 Erlangen, Germany
[b] Zienkiewicz Centre for Computational Engineering, College of Engineering, Bay Campus, Swansea University, Swansea, United Kingdom
[c] Mechanical & Industrial Engineering Department, New Jersey Institute of Technology, 200 Central Ave, Newark, NJ 07102, USA
[d] Glasgow Computational Engineering Centre (GCEC), University of Glasgow, United Kingdom

ARTICLE INFO

*Keywords:*
Dielectric elastomers
Electro-active polymers
Electro-mechanics
Particle filled polymers

ABSTRACT

A comprehensive experimental study performed under a combination of electro-mechanical loads on a particle-filled silicone as a representative of dielectric elastomers is presented in the Part I of this work (Mehnert et al., submitted, 2021). The constitutive modeling and numerical simulation of electro-active polymers are essential fields of research in order to increase the acceptance of this group of soft smart materials in real-life applications. However, only few contributions containing constitutive modeling approaches are combined with experimental data obtained from electro-mechanically coupled loading conditions due to the complexity of corresponding experiments. In this contribution, we aim to develop an electro-mechanically coupled model, which closely replicates the response of a silicone polymer filled with a high dielectric permittivity filler of varying fractions that are characterized under a combination of electric and mechanical loads. Once the model is calibrated with the experimental data described in Part I of this contribution, it is used for a simple illustrative application example showcasing the capability of the model and the influence of the different material characteristics.

## 1. Introduction

The term electro-active polymers (EAPs), defines a wide range of soft materials that have the ability of undergoing large deformations under excitation by an electric field (Carpi, 2010). This subclass of smart materials shows great potential as soft artificial muscles (Bar-Cohen, 2004) thanks to their inherent mechanical properties. Furthermore, in various other potential applications such as stretchable sensors, flexible generators or flexible optics (O'Halloran et al., 2008; Bar-Cohen, 2002; Collins et al., 2021; Vertechy et al., 2014; Böse and Fuß, 2014; Koh et al., 2011), the use of EAPs shows great promise. Prominent examples of EAPs are the so-called dielectric elastomers (DEs) that are especially popular as they are relatively easy to manufacture and simple to handle. These can be used for the design of soft actuators by the addition of flexible electrodes on both sides of a thin polymeric layer. Upon the application of an electric potential difference between the electrodes, the sample contracts in the thickness direction while simultaneously expanding in the lateral directions due to the attractive forces between the oppositely charged electrodes. The extent to which an actuator will deform is determined by the mechanical and dielectric properties of the underlying soft polymer. While classical polymeric materials such as silicones or acrylates display necessary soft mechanical properties, these materials usually do not inherit specifically high dielectric constants and thus do not have favorable dielectric properties that are needed to induce the required forces from an externally applied electric field. A well-known concept for optimizing the dielectric properties is the addition of filler particles with high dielectric constant, such as Barium-Titanate, Titanium Oxides, carbon nanotubes, etc that enhance the overall electro-mechanical performances of the composites as demonstrated in Part I of this publication series.

In order to widen the applications and acceptance of EAP-based compounds, computational modeling approaches become indispensable tools in predicting the material response under a combined electro-mechanical loading. For predicting the purely mechanical response of particle filled polymeric materials, mathematical models used in computer-based simulations have been developed over the past years that were initially restricted to small deformations (Guth, 1945) and later extended accounting for large deformations based on finite strain theories, see Bergstrom and Boyce (1999). Furthermore, in an effort

* Corresponding author.
*E-mail addresses:* markus.mehnert@fau.de (M. Mehnert), jessica.faber@fau.de (J. Faber), mokarram.hossain@swansea.ac.uk (M. Hossain), shawn.a.chester@njit.edu (S.A. Chester), paul.steinmann@fau.de (P. Steinmann).

https://doi.org/10.1016/j.euromechsol.2022.104661
Received 19 January 2022; Received in revised form 31 March 2022; Accepted 10 May 2022
Available online 4 June 2022

to incorporate the rate-dependent behavior of particle filled polymers, various phenomenological models were developed using the concept of so-called stress-like internal variables for which suited evolution equations are required (Kaliske and Rothert, 1997; Holzapfel and Simo, 1996; Wang and Chester, 2018). While these models considered the effective material as homogeneous, multiscale models such as (Zeng et al., 2008) approached the topic by also investigating the behavior on the microscale, in which the particles and the polymeric base material can clearly be distinguished.

For developing mathematical models that can replicate electro-responsive material behavior, electro-mechanically coupled constitutive approaches were developed based on the interplay between a deforming body and an electric field, see the seminal works, e.g., by Eringen (1963) or Toupin (1956). These ground-laying works have been expanded over the last decades especially sparked by the growing interests in electro-active soft polymeric materials (Kovetz, 2000; Ericksen, 2007; Dorfmann and Ogden, 2005; Ask et al., 2012). These concepts were also extended to so-called multiscale homogenization approaches, e.g. in the works by Schröder and Keip (2012) and Keip et al. (2014) where two-scale homogenization methods are used for the solution of the electro-mechanical problem. Similarly, in a series of papers Lopez-Pamies et al. derived a homogenization method for dielectric composites capable of replicating the purely mechanical response of filled polymers and their electro-mechanical behavior (Lopez-Pamies, 2014; Lefèvre and Lopez-Pamies, 2017a,b; Lefevre and Lopez-Pamies, 2017; Francfort et al., 2021; Ghosh et al., 2019) validated by experimental data presented in Huang et al. (2005). In these works, special attention was put on the influence of particle interphases and the role of space charges on the material response.

Within the scope of the current work, we combine these concepts for the simulation of the electro-mechanical behavior of a particle filled silicone. To this end, a number of experiments were performed under electro-mechanical loads in order to characterize the material response of the silicone Elastosil P 7670$^{TM}$ filled with Barium-Titanate particles, see Part I of this publication series. Based on the obtained results, the material parameters of the presented model are identified resulting in a comprehensive constitutive model of the composite material under combined mechanical and electric loading.

This contribution is structured as follows. In Section 2 the general modeling approach is introduced. In the following Section, the experimental results and the modeling approach are combined in order to identify the necessary mechanical and electro-mechanical material parameters. In order to illustrate the material characteristics, a simple numerical application example is presented in Section 4. Finally, Section 5 presents a brief summary of this contribution and an outlook.

## 2. Constitutive modeling

In this section, an electro-mechanical modeling approach is presented and specified with suitable terms from the literature. The model is developed in such a way that the material behavior of both unfilled and particle filled silicones can be replicated as closely as possible with the experimental data produced in Part I of this contribution. Our prime aim is to reduce the number of material parameters appearing in the model to a minimum. However, the complexity of the observed responses results in an extensive format of the final expressions. As typical for other polymers, we assume that the underlying response of the unfilled silicone studied here is viscoelastic. However, by comparing the data obtained from the multistep relaxation tests and the cyclic loading tests with a very slow stretch rate ($\dot{\lambda} = 0.01\ \mathrm{s}^{-1}$), we observe that there is a rate-independent difference between the loading and the unloading curves. Furthermore, we can clearly identify a residual strain at the end of the deformation cycle. As the material samples were preconditioned, we do not consider this phenomenon as a consequence of the so-called Mullins effect, describing a unique and permanent softening of the material after the first deformation. Instead, we conjecture that in order to describe the observed material response, the classical elastic behavior has to be augmented to a pseudo-elastic material response as introduced in Ogden and Roxburgh (1999) , which has been used for the modeling of residual strains in different soft materials (Fung et al., 1979; Ogden, 2003). Therefore, this formulation is subsequently extended to viscoelasticity which captures the behavior of the base material. Such an approach is similar to the combination of viscoelasticity and stress-softening as presented by Wang and Chester (2018). The addition of filler particles alters both the elastic and viscous behavior, thus both energy contributions will be modified accordingly. Finally, the energy function has to be extended by electro-mechanical coupling terms that reflect the capability of the dielectric to deform under the application of an electric field. This combination of different material characteristics is summarized in Fig. 1, showcasing the corresponding curves from the conducted experiments that characterize the specific material behavior.

Generally, we distinguish in our modeling approach between the response of the unfilled silicone (upper plots of Fig. 1) and the particle filled compound (lower plots of Fig. 1) where we assume that the unfilled material is the foundation that is subsequently extended. The underlying elastic material response of a pure silicone is modified to pseudo-elasticity in order to replicate the rate-independent hysteresis, visible in the upper central plot in Fig. 1. Additionally, a rate-dependent response of the material is visible at increased strain rates as shown in the upper right plot. Consequently, the model is further extended to pseudo-viscoelasticity. Upon the addition of the stiffer particles, the material behavior noticeably changes. As shown in the plot on the lower left side, the underlying elasticity stiffens with the increasing particle concentration. This is accounted for by the modification of the elastic material model. Furthermore, the filler particles lead to an increase in the dissipated energy. Thus, the viscoelastic description of the material is modified. At this point, the mechanical response of the material is completed and this filler-content dependent pseudo-viscoelastic material model is extended to an electro-mechanically coupled form.

We assume the existence of an energy function $W$ that can be used to derive the mechanical and electric quantities describing the material behavior. This energy function can be decomposed into a volumetric contribution $W_{vol}$ and an isochoric contribution $W_{iso}$. The former describes the volume changing deformation whereas the latter describes the volume preserving part of the deformation. As we assume that the material under consideration shows incompressible response, the volumetric energy contribution vanishes and will not be addressed further in the following. Therefore, we can state that $W = W_{iso}$. Following the structure of the conducted experiments, we will extend and modify the expression stepwise to describe the material characteristics.

### 2.1. Constitutive modeling of the mechanical response of unfilled silicone

Initially, it is assumed that the energy function $W$ consists of an elastic contribution $W^{el}$ and a viscous contribution $W^{v}$. For modeling purely elastic response of a polymeric material, a wide range of well established energy functions can be found in the literature (Hossain and Steinmann, 2013). However, in the current case, a rate-independent hysteresis can be observed that would not be replicated by a strictly elastic approach. Consequently, a pseudo-elastic description is adopted from (Ogden and Roxburgh, 1999) resulting in an elastic energy contribution that reads as

$$W^{el}(\overline{\boldsymbol{C}}) = \eta_1 W_0^{el}(\overline{\boldsymbol{C}}) + [1-\eta_2]N(\overline{\boldsymbol{C}}). \tag{1}$$

Here we introduce an elastic base function $W_0^{el}(\overline{\boldsymbol{C}})$ that is formulated in terms of the isochoric part of the right Cauchy–Green tensor defined as $\overline{\boldsymbol{C}} = \boldsymbol{J}^{-2/3}\boldsymbol{F}^T \cdot \boldsymbol{F}$ with the deformation gradient $\boldsymbol{F}$ and its Jacobian $\boldsymbol{J} = \det \boldsymbol{F}$. In the current study, a Yeoh-type energy formulation is selected that reads

$$W_0^{el}(\overline{\boldsymbol{C}}) = c_1^{el}\left[\overline{I}_1 - \dim\right] + c_2^{el}\left[\overline{I}_1 - \dim\right]^2 + c_3^{el}\left[\overline{I}_1 - \dim\right]^3 \tag{2}$$

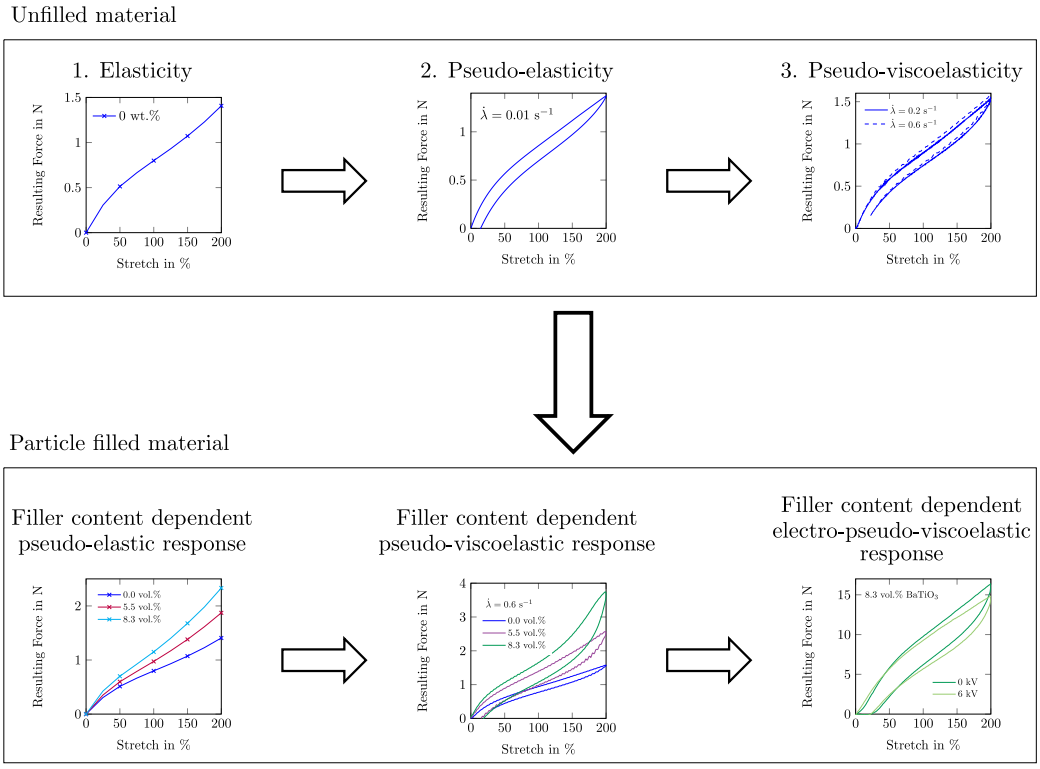


**Fig. 1.** A summary of the key structure of the different material characteristics under consideration.

For identifying the elastic material parameters $c_i^{el}$ $(i = 1,2,3)$, experimental data obtained from the multistep relaxation tests of pure Elastosil will be used. Note that the first invariant of the right Cauchy–Green tensor is defined as $\overline{I}_1 = \overline{\boldsymbol{C}} : \boldsymbol{I}$, where $\boldsymbol{I}$ is the identity tensor. This base function is extended by the two parameters $\eta_1$ and $\eta_2$ as well as the function $N(\overline{\boldsymbol{C}})$ that captures the rate-independent hysteresis and the residual strain. These parameters will be either active or inactive depending on the course of the deformations. While a sample material is loaded, it is assumed that $\eta_1 = 1$ and $\eta_2 = 1$, whereas they can take different values during unloading. We follow the notion given in Dorfmann and Ogden (2004) and define $N(\overline{\boldsymbol{C}})$ as

$$N(\overline{\boldsymbol{C}}) = \frac{1}{2}\left[\upsilon_1\left[\overline{\lambda}_1^{-2} - 1\right] + \upsilon_2\left[\overline{\lambda}_2^{-2} - 1\right] + \upsilon_3\left[\overline{\lambda}_3^{-2} - 1\right]\right] \tag{3}$$

which corresponds to a modified Neo-Hookean formulation with the material parameters $\upsilon_i$ $(i = 1,2,3)$ and the principal isochoric stretches $\overline{\lambda}_i$. By the definition of the material parameters as

$$\begin{aligned} \upsilon_1 &= \mu\left[1 - \frac{1}{3.5}\tanh(10[\lambda_m - 1])\right], \\ \upsilon_2 &= \upsilon_3 = \mu \end{aligned} \tag{4}$$

the effect of a residual strain is introduced. The formulations contain a material parameter $\mu$ with a further dependency on the maximum strain $\lambda_m$ in the loading direction. The parameters $\eta_1$ and $\eta_2$ from Eq. (1) are defined as

$$\begin{aligned} \eta_1 &= 1 - \frac{1}{r}\tanh\left(\frac{W_m^{el}(\overline{\boldsymbol{C}}_m) - W_0^{el}(\overline{\boldsymbol{C}})}{\mu m}\right), \\ \eta_2 &= \tanh\left(\left[W_0^{el}(\overline{\boldsymbol{C}})/W_m^{el}(\overline{\boldsymbol{C}}_m)\right]^{\alpha\left(W_m^{el}(\overline{\boldsymbol{C}}_m)\right)}\right)/\tanh(1), \\ \alpha &= a + bW_m^{el}(\overline{\boldsymbol{C}}_m)/\mu, \end{aligned} \tag{5}$$

where $W_m^{el}(\overline{\boldsymbol{C}}_m)$ is the elastic energy at the maximum applied deformation $\overline{\boldsymbol{C}}_m$ and the parameters $r$, $m$, $a$ and $b$ have to be identified using the results of the cyclic loading experiments performed at the slowest stretch rate.

On the top of this, apparent changes in the stress–strain curve in response to a change in the deformation rate are attributed to a viscous contribution to the response of the unfilled material. Thus, the viscous contribution $W^v$ is added to the energy function initially depending on the deformation described by the right Cauchy–Green tensor and a set of internal variables $\boldsymbol{A}_i$, i.e.,

$$W^v(\overline{\boldsymbol{C}}, \boldsymbol{A}_i) = \sum_i W_i^v(\overline{\boldsymbol{C}}, \boldsymbol{A}_i). \tag{6}$$

In order to describe the complex time-dependent behavior of the material, the viscous energy consists of a number of functions $W_i^v(\overline{\boldsymbol{C}}, \boldsymbol{A}_i)$ $(i = 1,2,3...)$, each of which represents a viscous Maxwell element. For the description of the response of pure Elastosil, we assume three viscous functions, the first two of which are defined as a Neo-Hookean type. In combination with the evolution equations that determine the internal variables, these read

$$\begin{aligned} W_i^v(\overline{\boldsymbol{C}}, \boldsymbol{A}_i) &= \frac{1}{2}\sum_i \mu_i^v\left[\overline{I}_{1,i}^v - \dim\right], \\ \dot{\boldsymbol{A}}_i &= \frac{1}{\tau_i}\left[\overline{\boldsymbol{C}} - \frac{1}{\dim}\overline{I}_{1,i}^v \boldsymbol{A}_i\right], \end{aligned} \tag{7}$$

with $i = 1,2$. Here, the viscous shear moduli $\mu_i^v$ are introduced while the viscous invariants are defined as $\overline{I}_{1,i}^v = \boldsymbol{A}_i^{-1} : \overline{\boldsymbol{C}}$. The final contribution and its corresponding evolution law are formulated as a Yeoh-type function that reads

$$\begin{aligned} W_3^v(\overline{\boldsymbol{C}}, \boldsymbol{A}_3) &= c_1^v\left[\overline{I}_{1,3}^v - \dim\right] + c_2^v\left[\overline{I}_{1,3}^v - \dim\right]^2 + c_3^v\left[\overline{I}_{1,3}^v - \dim\right]^3, \\ \dot{\boldsymbol{A}}_3 &= \left[\frac{1}{\tau_{3,1}} + \frac{2\left[\overline{I}_{1,3}^v - \dim\right]}{\tau_{3,2}} + \frac{3\left[\overline{I}_{1,3}^v - \dim\right]^2}{\tau_{3,3}}\right]\left[\overline{\boldsymbol{C}} - \frac{1}{3}\overline{I}_{1,3}^v \boldsymbol{A}_3\right]. \end{aligned} \tag{8}$$

It should be noted that the relaxation times $\tau_{3,i}$ $(i = 1,2,3)$ are defined as $\tau_{3,i} = \tau_3/c_i^v$. These expressions are derived in a thermodynamically

consistent way following the approach outlined in Koprowski-Theiss et al. (2011). The viscous material parameters $\mu_i$, $c_i^v$ and $\tau_i$ $(i = 1, 2, 3)$ have to be identified using the cyclic loading data obtained from tests performed at higher deformation rates.

### 2.2. Constitutive modeling of the mechanical response of particle filled silicone

As observed in the experimental data, the addition of filler particles leads to modifications of both the elastic and the viscous responses of the dielectric elastomers. In the case of the elastic energy contribution $W^{el}(\overline{\boldsymbol{C}})$, these changes can be incorporated by introducing a modified invariant $\widetilde{I}_1^e$ following the approach presented in Bergstrom and Boyce (1999), which reads

$$\widetilde{I}_1^e = \left[1 + g_1^{el} v_f + \left[g_2^{el} v_f\right]^2\right]\left[\overline{I}_1 - \mathrm{dim}\right] + \mathrm{dim} = X_{el}\left[\overline{I}_1 - \mathrm{dim}\right] + \mathrm{dim}, \quad (9)$$

where $v_f$ describes the filler content of the material and $g_1^e$ and $g_2^e$ are material parameters. The modified form of the elastic base energy from Eq. (2) is labeled as $\widetilde{W}_0^{el}(\overline{\boldsymbol{C}})$ and reads

$$\widetilde{W}_0^{el}(\overline{\boldsymbol{C}}) = c_1^{el}\left[\widetilde{I}_1 - \mathrm{dim}\right] + c_2^{el}\left[\widetilde{I}_1 - \mathrm{dim}\right]^2 + c_3^{el}\left[\widetilde{I}_1 - \mathrm{dim}\right]^3. \quad (10)$$

Similar to the elastic part of the energy, the viscous contributions need modifications in order to capture the influence of the filler particles. The results of the cyclic loading tests show an increase in the stiffness of the material and a change in the form of the hysteresis curves originating from the addition of the fillers. Consequently, in addition to the introduction of a modified first invariant $\widetilde{I}_{1,i}^v$ $(i = 1, 2, 3)$ and material parameters $g_1^v$ and $g_2^v$, a modification for each of the relaxation times $\tau_i$ $(i = 1, 2, 3)$ with a quadratic scaling function is introduced, i.e.,

$$\begin{aligned}\widetilde{I}_{1,i}^v &= \left[1 + g_1^v v_f + \left[g_2^v v_f\right]^2\right]\left[\overline{I}_{1,i}^v - \mathrm{dim}\right] + \mathrm{dim} = X_v\left[\overline{I}_{1,i}^v - \mathrm{dim}\right] + \mathrm{dim},\\ \widetilde{\tau}_i &= \left[1 + g_{1,i}^\tau v_f + \left[g_{2,i}^\tau v_f\right]^2\right]\tau_i = X_{\tau,i}\tau_i.\end{aligned} \quad (11)$$

It should be noted that the model parameters introduced here are responsible for the increase in the magnitude of the combined viscoelastic stress response and the amount of the energy dissipation. However, due to the complex interplay of the different Maxwell elements, a direct relation of each parameter to the form of the hysteresis is not possible. When these modifications are implemented into Eqs. (7) and (8), the first two member functions take the form

$$\begin{aligned}\widetilde{W}_i^v(\overline{\boldsymbol{C}}, \boldsymbol{A}_i) &= 0.5\sum_i \mu_i^v\left[\widetilde{I}_{1,i}^v - \mathrm{dim}\right],\\ \dot{\boldsymbol{A}}_i &= \frac{1}{\widetilde{\tau}_i}\left[\overline{\boldsymbol{C}} - \frac{1}{\mathrm{dim}}\widetilde{I}_{1,i}^v \boldsymbol{A}_i\right],\end{aligned} \quad (12)$$

whereas the final contribution reads

$$\begin{aligned}\widetilde{W}_3^v(\overline{\boldsymbol{C}}, \boldsymbol{A}_3) &= c_1^v\left[\widetilde{I}_{1,3}^v - \mathrm{dim}\right] + c_2^v\left[\widetilde{I}_{1,3}^v - \mathrm{dim}\right]^2 + c_3^v\left[\widetilde{I}_{1,3}^v - \mathrm{dim}\right]^3,\\ \dot{\boldsymbol{A}}_3 &= \left[\frac{1}{\widetilde{\tau}_{3,1}} + \frac{2\left[\widetilde{I}_{1,3}^v - \mathrm{dim}\right]}{\widetilde{\tau}_{3,2}} + \frac{3\left[\widetilde{I}_{1,3}^v - \mathrm{dim}\right]^2}{\widetilde{\tau}_{3,3}}\right]\left[\overline{\boldsymbol{C}} - \frac{1}{3}\widetilde{I}_{1,3}^v \boldsymbol{A}_3\right].\end{aligned} \quad (13)$$

In summary, the effect of the addition of filler particles on the mechanical response is modeled by eight modified parameters that have to be identified using the experimental results.

### 2.3. Constitutive modeling of the electro-mechanical response of particle filled silicone

Finally, coupling of the electric field with the mechanical response needs to be established. Within the data available in the current study, it is difficult to distinguish between the effects of the electric field on the elastic and the viscous parts of the material response. Hence, it is assumed that only the elastic energy contribution is dependent on the electric field. Such a simplification brings extra advantage as every additional electro-mechanical coupling parameter introduced here results in a considerable increase in the runtime of the optimization routine later on. Therefore, in order to keep the material parameters at a minimum, the electric coupling in the elastic energy contribution is introduced by modifications of the coupling invariant $\overline{I}_5$ and the dominating first material parameter $c_1^e$. Note that the viscous energy contributions are kept unchanged which renders the respective energy functions into the format

$$\begin{aligned}&\widetilde{W}_0^{el}(\overline{\boldsymbol{C}}_{\mathrm{EM}}, \mathbb{E}) =\\ &\quad c_1^{el}(I_4)\left[\widetilde{I}_1 - \mathrm{dim}\right] + c_2^{el}\left[\widetilde{I}_1 - \mathrm{dim}\right]^2 + c_3^{el}\left[\widetilde{I}_1 - \mathrm{dim}\right]^3 + \gamma_2\widetilde{I}_5.\end{aligned} \quad (14)$$

Here we have introduced the fifth invariant $I_5 = [\mathbb{E} \otimes \mathbb{E}] : \overline{\boldsymbol{C}}$ that depends on the electric field that is defined as the material gradient of an electric potential $\varphi$ as $\mathbb{E} = -\mathrm{Grad}\varphi$. For a more detailed introduction of the electro-mechanical basics, reader is referred to Mehnert et al. (2016), Steinmann (2011), Mehnert et al. (2016) and Dorfmann and Ogden (2006). As is observed from the experimental data, the inclusion of filler particles increases the electro-mechanical coupling, hence, the field sensitive coupling parameters are modified via the particle concentration $v_f$ in the form

$$c_1^{el}(I_4) = \hat{c}_1^{el} - [1 + k v_f]\beta^e I_4, \quad \gamma = [1 + k v_f]\hat{\gamma}, \quad (15)$$

where a fourth invariant $I_4 = [\mathbb{E} \otimes \mathbb{E}] : \boldsymbol{I}$ is introduced. The above equations convey the notion that the material has a zero field ground state captured by the parameter $\hat{c}_1$. This parameter is further influenced by the application of an electric field that can be scaled by the coupling parameters $\beta^e$ and a factor $k$ incorporating the concentration of the filler particles. Similarly, the coupling parameter $\gamma_2$ is also scaled by $v_f$ in order to take into account the influence of increasing filler concentrations. Finally, in order to incorporate a field sensitivity of the elastic contribution, the pseudo-elasticity function $N(\overline{\boldsymbol{C}})$ is also modified into a field sensitive form. This is achieved by changing the material parameter $\mu$ introduced in Eq. (4) into an expression $\widetilde{\mu}(I_4)$ that reads

$$\widetilde{\mu}(I_4) = \hat{\mu} - [1 + 5 k v_f]\beta^e I_4. \quad (16)$$

Thus, three additional material parameters have to be identified using the results of the electro-mechanically coupled experiments in order to characterize the coupling behavior of the particle-filled silicone. Table 1 presents a summary of all 29 necessary material parameters appearing in the electro-mechanical modeling framework.

## 3. Parameter identification

In the following section, a material parameter identification process using the data obtained from the electro-mechanical experiments is described. This is done by calculating the resulting force over the course of a specific experiment and fitting this solution to the experimental results. We follow the same logic as in the previous chapter that proposes a modular structure of the constitutive framework. Consequently, the identification process starts by first finding the elastic, pseudo-elastic, and viscous material parameters of unfilled silicone, followed by the identification of the parameters describing the influence of the filler particles on the elastic and viscous material responses. In these cases, an analytical solution to the experiments can be calculated due to the selected sample geometry. Finally, the electro-mechanical coupling parameters are identified. However, due to the non-homogeneous sample deformation in these coupled experiments, the tests cannot be assumed to be uniaxial and therefore, no analytical solution can be calculated. Thus, a numerical solution is obtained using a finite element implementation of the derived modeling approach which is fitted to the experimental data.

For the identification of the mechanical parameters, the stress state during the conducted experiments can be calculated analytically. For

**Table 1**
A summary of the 29 material parameters of the modeling approach for Elastosil P 7670™ filled with $BaTiO_3$ particles. Parameters $c_i$, $\mu_i^v$ in N/mm$^2$, $\tau_i$ in s, $\beta^e$ in N/(Vmm)$^2$, $\hat{\gamma}_2$ in N/V$^2$.

| | | | | | | | |
|---|---|---|---|---|---|---|---|
| **Elastosil P 7670™ filled with $BaTiO_3$ particles** | | | | | | | |
| **Mechanical Base Parameters** | | | | | | | |
| Elastic Parameters | | | | | | | |
| $\hat{c}_1^{el}$ | | | $c_2^{el}$ | | | | $c_3^{el}$ |
| Pseudo-Elastic Parameters | | | | | | | |
| $\hat{\mu}$ | | $r$ | | $m$ | | $a$ | $b$ |
| Viscous Parameters | | | | | | | |
| $\mu_1^v$ | | $\mu_2^v$ | | $c_1^v$ | | $c_2^v$ | $c_3^v$ |
| $\tau_1$ | | $\tau_2$ | | | | $\tau_3$ | |
| **Particle Scaling Parameters** | | | | | | | |
| Elastic Scaling Parameters | | | | | | | |
| $g_1^e$ | | | $g_2^e$ | | | | |
| Viscous Scaling Parameters | | | | | | | |
| $g_1^v$ | $g_2^v$ | $g_{1,1}^\tau$ | $g_{2,1}^\tau$ | $g_{1,2}^\tau$ | $g_{2,2}^\tau$ | $g_{1,3}^\tau$ | $g_{2,3}^\tau$ |
| **Electro-Mechanical Coupling Parameters** | | | | | | | |
| $\beta^e$ | | | $\hat{\gamma}_2$ | | | | $k$ |

this, we introduce the Piola–Kirchhoff stress tensor $\boldsymbol{S}$ as the derivative of the energy function with respect to the right Cauchy–Green tensor, i.e.,

$$\boldsymbol{S} = 2\frac{\partial W(\overline{\boldsymbol{C}}, \boldsymbol{A}_i, \mathbb{E})}{\partial \boldsymbol{C}}. \tag{17}$$

Here, the most general case is assumed considering that a particle filled silicone may be put under both mechanical and electric loads. In this context, it is usually convenient to introduce the isochoric version of the Piola–Kirchhoff tensor as $\overline{\boldsymbol{S}} = 2\partial W(\overline{\boldsymbol{C}}, \boldsymbol{A}_i, \mathbb{E})/\partial \overline{\boldsymbol{C}}$ that we can transform into the conventional Piola–Kirchhoff stress $\boldsymbol{S}$ with the help of $\mathbb{P} = \partial \overline{\boldsymbol{C}}/\partial \boldsymbol{C}$, the fourth-order projection tensor. We can decompose this stress tensor further into an elastic part $\overline{\boldsymbol{S}}^{el}$ and a viscous part $\overline{\boldsymbol{S}}^{v}$. In order to compare these stresses to the obtained data curves, we introduce the Piola stress tensor $\boldsymbol{P}$ which is linked to $\boldsymbol{S}$ via

$$\boldsymbol{P} = \boldsymbol{F} \cdot [\overline{\boldsymbol{S}}^{el} + \overline{\boldsymbol{S}}^{v}] : \mathbb{P} = \boldsymbol{F} \cdot [\boldsymbol{S}^{el} + \boldsymbol{S}^{v}]. \tag{18}$$

Following the classical assumption, the polymer studied here is considered as an incompressible material. Furthermore, for the case of purely mechanical experiments, the stress state inside a sample is homogeneous due to the selected sample geometry. Thus, the deformation gradient $\boldsymbol{F}$ and the corresponding right Cauchy–Green tensor $\boldsymbol{C}$ for the case of uniaxial stretching read

$$\boldsymbol{F} = \begin{bmatrix} \lambda & 0 & 0 \\ 0 & \lambda^{-1/2} & 0 \\ 0 & 0 & \lambda^{-1/2} \end{bmatrix}, \quad \boldsymbol{C} = \begin{bmatrix} \lambda^2 & 0 & 0 \\ 0 & \lambda^{-1} & 0 \\ 0 & 0 & \lambda^{-1} \end{bmatrix}. \tag{19}$$

Here, we define $\lambda$ as $\lambda = [L_0 + \Delta L]/L_0$, the ratio between the extended length $L_0 + \Delta L$ and the initial length of the sample $L_0$. Consequently, the stretch rate is defined as $\dot{\lambda} = \dot{\Delta L}/L_0$. The stretch-like internal variables $\boldsymbol{A}_i$ take a form resembling $\boldsymbol{C}$, i.e.,

$$\boldsymbol{A}_i = \begin{bmatrix} A_i^2 & 0 & 0 \\ 0 & A_i^{-1} & 0 \\ 0 & 0 & A_i^{-1} \end{bmatrix}. \tag{20}$$

In the following sections, this form of the deformation gradient is inserted into the definition of the stress in order to compare the experiments with the analytical solution.

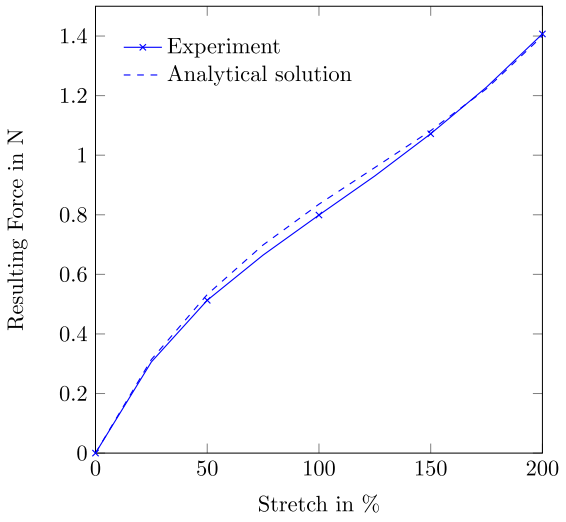


**Fig. 2.** Calibration of the analytical solution (dashed line) to the experimental results (solid line) of the resulting equilibrium force values obtained from a multi-step relaxation test of unfilled Elastosil P 7670™.

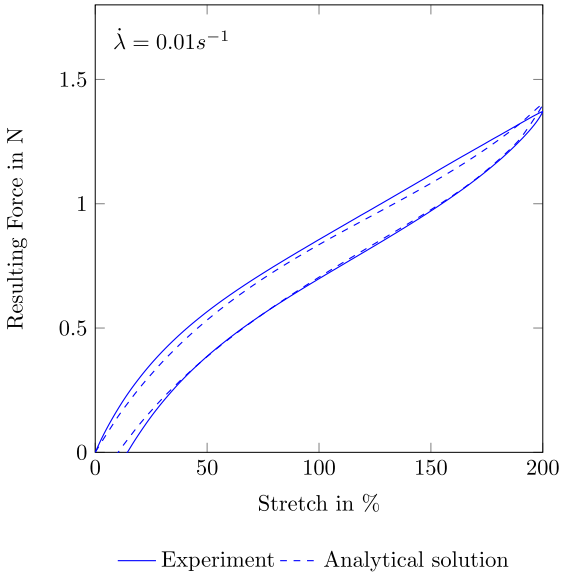


**Fig. 3.** Comparison between the experimental results (solid line) and the analytical solution (dashed) of cyclic loading–unloading tests performed with unfilled Elastosil P 7670™ with $\dot{\lambda} = 0.01\ s^{-1}$. (Pseudo-elastic material behavior).

### 3.1. Identification of the mechanical parameters of unfilled silicone

At first, the elastic base parameters $c_i^{el}$ from Eq. (2) are identified by fitting the analytical solution of the equilibrium curve to the corresponding experimental data. In this case, we assume that the recorded data can be attributed to the purely elastic material response. Thus, the analytical solution that is fitted to the experimental results reads

$$\boldsymbol{P}^{el} = \frac{4}{3}\left[c_1^{el} + 2c_2^{el}\left[\lambda^2 + 2\lambda^{-1} - 3\right] + 3c_3^{el}\left[\lambda^2 + 2\lambda^{-1} - 3\right]^2\right]\left[\lambda - \lambda^{-2}\right]. \tag{21}$$

Note that in the aforementioned equation, the first elastic parameter is labeled as $c_1^{el}$. In the electro-mechanical case, where this term is scaled with the electric field, parameter $c_1^{el}$ corresponds to the base parameter $\hat{c}_1^{el}$. For the purely mechanical case at present, however, the additional circumflex accent is omitted for the sake of readability. The fit of the analytical solution to the equilibrium curve is shown in Fig. 2, with

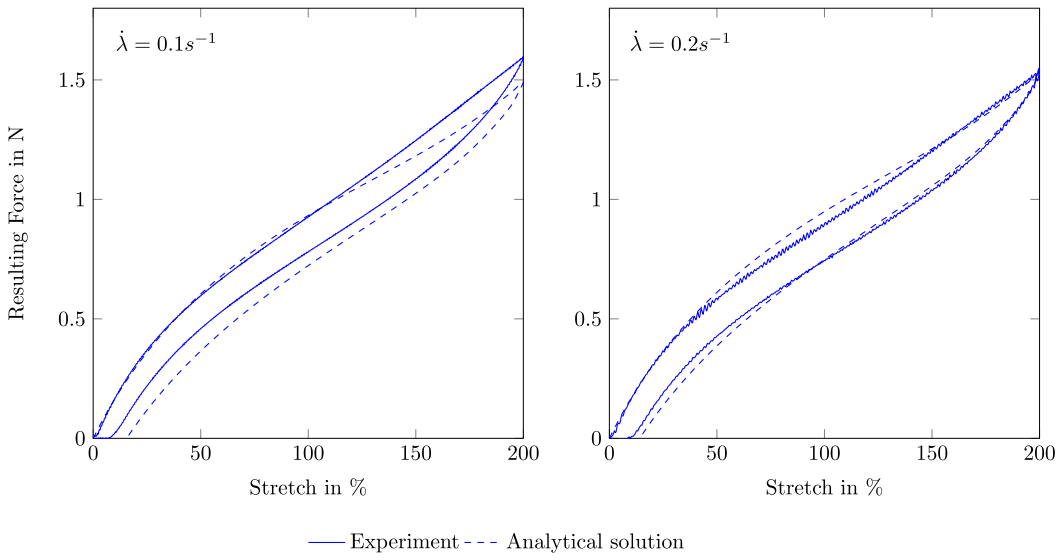


(a) Loading-unloading test with $\dot{\lambda} = 0.1$ s$^{-1}$ and $\dot{\lambda} = 0.2$ s$^{-1}$ used for the calibration of the model

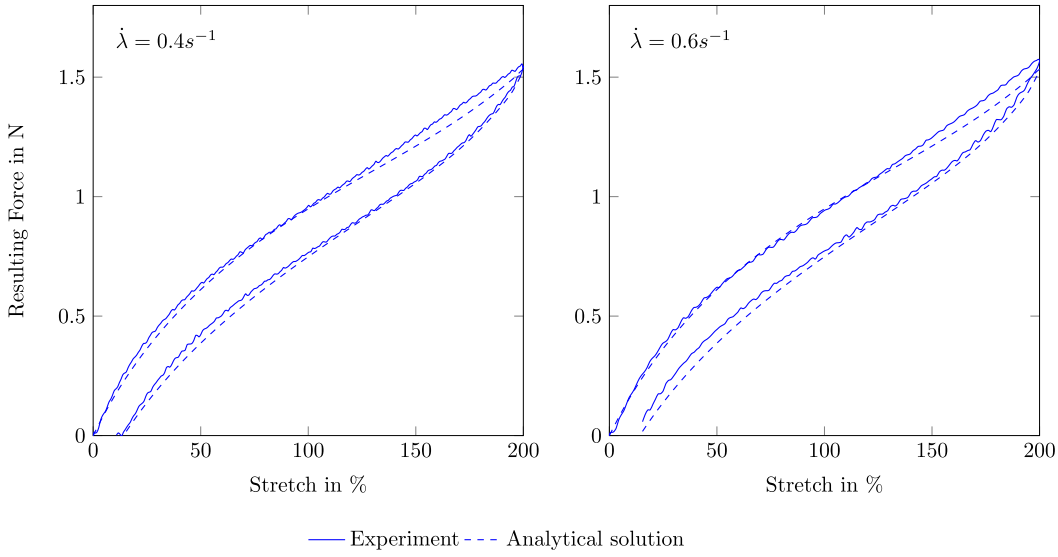


(b) Loading-unloading test with $\dot{\lambda} = 0.4$ s$^{-1}$ and $\dot{\lambda} = 0.6$ s$^{-1}$ used for the calibration of the model

**Fig. 4.** Comparison between the experimental results (solid lines) and the analytical solution (dashed lines) of cyclic loading–unloading tests performed with unfilled Elastosil P 7670™.

the identified material parameters $c_1^{el} = 0.0458$ N/mm$^2$, $c_2^{el} = -0.0012$ N/mm$^2$ and $c_3^{el} = 9.9 \cdot 10^{-5}$ N/mm$^2$.

As was pointed out previously, the equilibrium curve corresponds to the loading path of the cyclic loading test with the slowest stretch rate ($\dot{\lambda} = 0.01$ s$^{-1}$). Thus, the unloading curve at this stretch rate is described by the additional terms in Eq. (1), i.e., the parameters $\mu, r$ and $m$ from Eqs. (4) and (5). Consequently, the analytical solution that is fitted to the experimental results is modified to

$$P^{el} = \frac{4}{3}\eta_1\left[c_1^{el} + 2c_2^{el}\left[\lambda^2 + 2\lambda^{-1} - \text{dim}\right] + 3c_3^{el}\left[\lambda^2 + 2\lambda^{-1} - \text{dim}\right]^2\right]\left[\lambda - \lambda^{-2}\right] + [1 - \eta_2][v_1\lambda - 0.5[v_2 + v_3]\lambda^{-2}]. \tag{22}$$

The optimization of this solution to the respective cyclic loading data leads to the fit as presented in Fig. 3 with the identified values $\mu = 1.5$, $r = 1.14$, and $m = 0.3427$.

We can now use the already identified pseudo-elastic parameters as a basis for the identification of the viscous parameters. Thus, the viscous stress $P^v$ originating from a Neo-Hookean type model in the stretch direction can be calculated as

$$\begin{aligned} P_i^v &= \frac{4}{3}\mu_i^v\left[\lambda A_i^2 - \lambda^{-2}A_i^{-1}\right], \\ \dot{A}_i &= \frac{1}{3\tau_i}\left[\lambda^2 A_i^{-1} - A_i^2\lambda^{-1}\right] \quad \text{with } i = 1, 2. \end{aligned} \tag{23}$$

However, Yeoh-type contribution takes the form

$$\begin{aligned} P_3^v &= \frac{4}{3}\left[c_1^v + 2c_2^v\left[\overline{I}_{1,3}^v - 3\right] + 3c_3^v\left[\overline{I}_{1,3}^v - 3\right]^2\right]\left[\lambda A_3^{-2} - \lambda^{-2}A_3\right], \\ \dot{A}_3 &= \left[\frac{1}{3\tau_{3,1}} + \frac{2}{3\tau_{3,2}}[\overline{I}_{1,3}^v - \text{dim}] + \frac{1}{\tau_{3,3}}[\overline{I}_{1,3}^v - \text{dim}]^2\right]\left[\lambda^2 A_3^{-1} - A_3^2\lambda^{-1}\right], \\ \text{with} \quad \overline{I}_{1,3}^v &= \lambda^2 A_3^{-2} + 2\lambda^{-1}A_3, \end{aligned} \tag{24}$$

The combination of the elastic and the viscous stresses can be fitted to multiple experimental data sets at the same time using a *simultaneous minimization* technique (Hossain et al., 2012; Linder et al., 2011; Amin et al., 2002) in order to identify the viscous material parameters of the

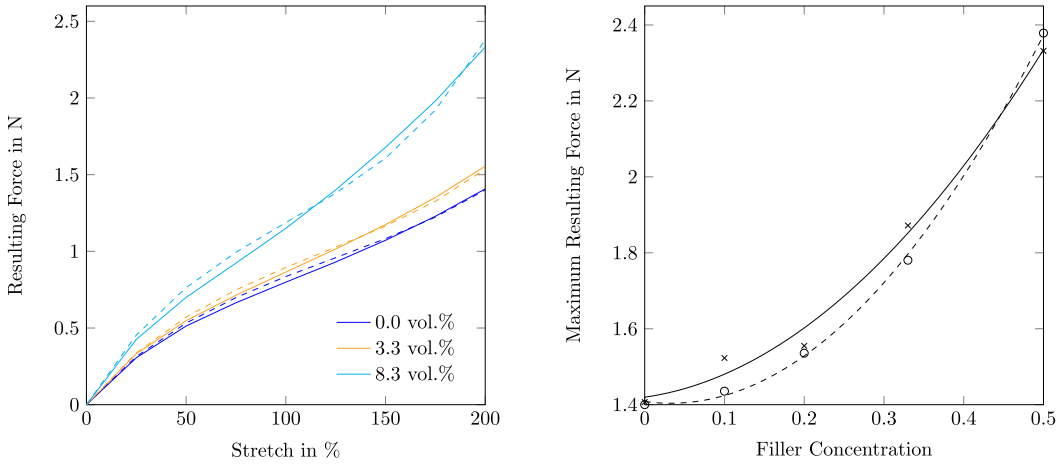


**Fig. 5.** Analytical solutions compared to experiments for the equilibrium values of the resulting force of multi-step relaxation tests for various filler concentrations. (Left) Analytical solution (dashed lines) and experimental values (solid lines) over the applied stretch, (right) simulation (o-marks and dashed trend line) and experimental values (x marks and solid line) of the resulting force for the maximum applied stretch over the range of tested filler concentrations.

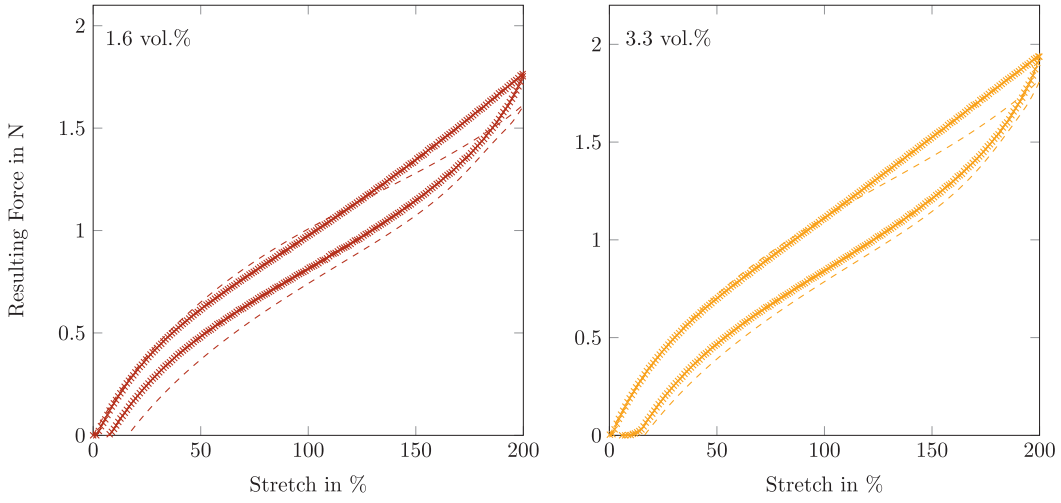


(a) Loading-unloading tests with filler contents of 1.6 vol.% and 3.3 vol.%

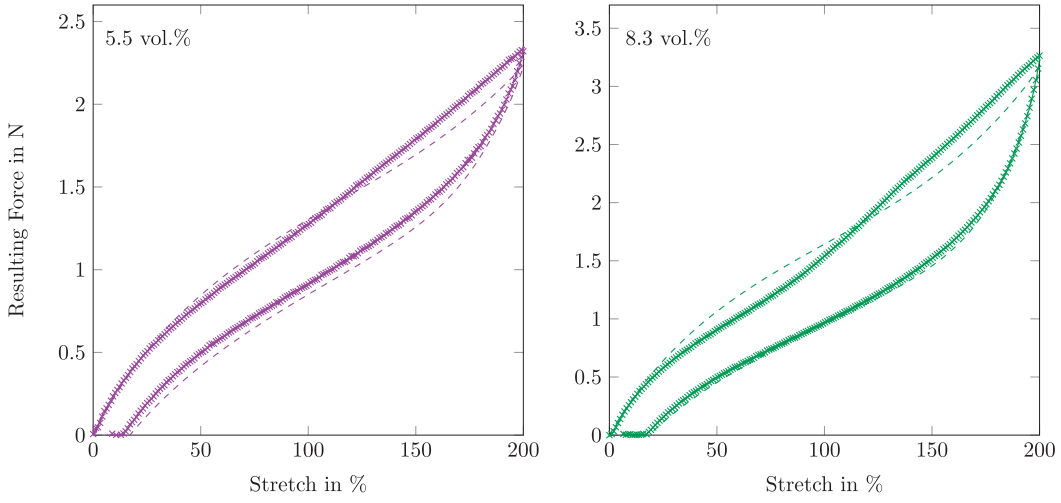


(b) Loading-unloading tests with filler contents of 5.5 vol.% and 8.3 vol.%

**Fig. 6.** Comparison between the experimental results (x-marks) and the simulation (dashed lines) of cyclic loading–unloading experiments for Elastosil P 7670™ with various filler contents at a stretch rate of 0.1 $s^{-1}$.

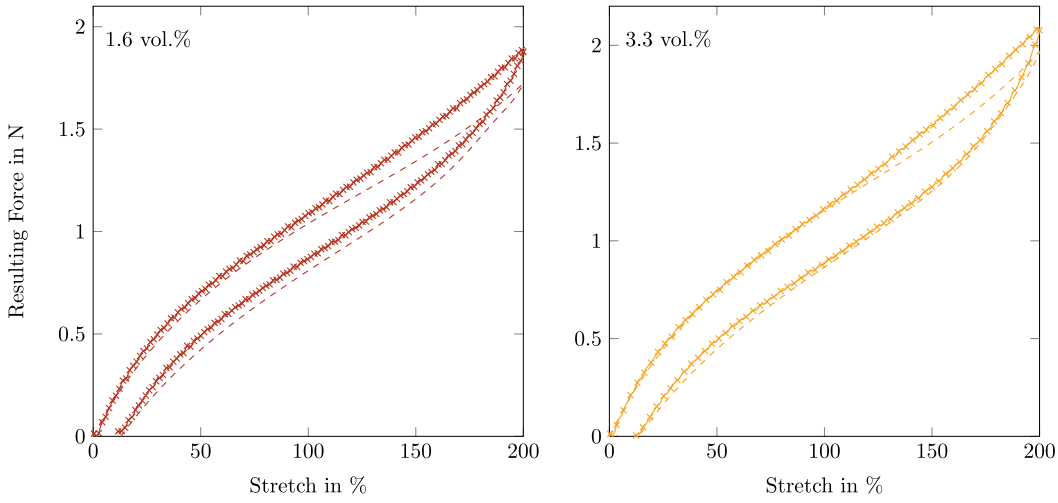


(a) Loading-unloading tests with filler fractions of 1.6 vol.% and 3.3 vol.%

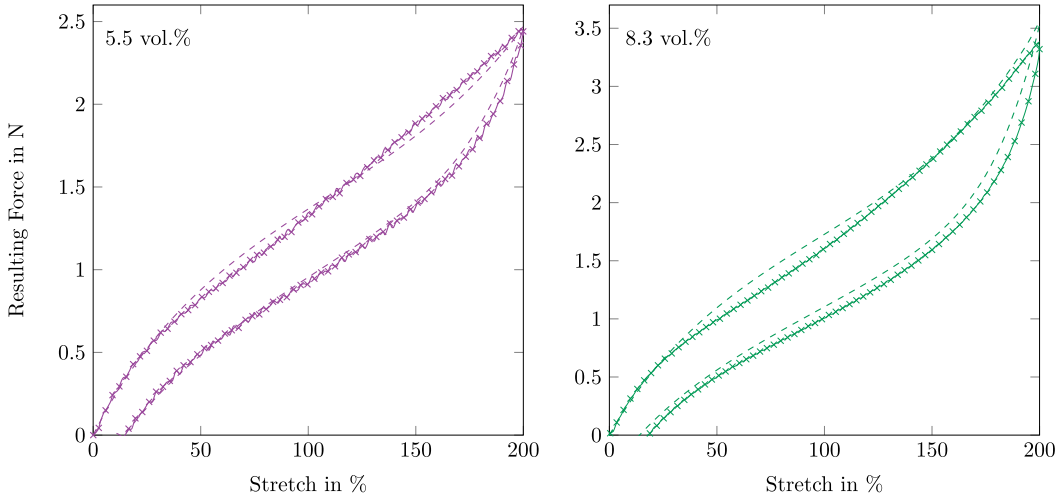


(b) Loading-unloading tests with filler fractions of 5.5 vol.% and 8.3 vol.%

**Fig. 7.** Comparison between the experimental results (x-marks) and the simulation (dashed lines) of cyclic loading–unloading experiments for Elastosil P 7670™ with various filler content at a stretch rate of 0.2 $s^{-1}$.

**Table 2**
Identified viscous material parameter sets for pure Elastosil P 7670™. $\mu_i^v$, $c_j^v$ in N/mm² and $\tau_i$ in s. Relaxation times $\tau_1$ and $\tau_2$ correspond to the Maxwell element modeled with a Neo-Hookean type formulation and the parameters $\mu_1^v$ and $\mu_2^v$. Relaxation time $\tau_3$ corresponds to the Maxwell element modeled with a Yeoh-type formulation and the parameters $c_i^v$.

| | | | | |
|---|---|---|---|---|
| $\mu_1^v$ | $\mu_2^v$ | $c_1^v$ | $c_2^v$ | $c_3^v$ |
| $4.14 \cdot 10^{-3}$ | $2.57 \cdot 10^{-3}$ | $6.51 \cdot 10^{-3}$ | $2.22 \cdot 10^{-14}$ | $4.04 \cdot 10^{-6}$ |
| $\tau_1$ | $\tau_2$ | $\tau_3$ | | |
| $4.39 \cdot 10^{-3}$ | 0.685 | 0.266 | | |

unfilled silicone. For this, the results of the experiments conducted with $\dot{\lambda} = 0.4\ s^{-1}$ and $\dot{\lambda} = 0.6\ s^{-1}$ are used as inputs for the optimization process, while the experimental data with the remaining stretch rates are used for the validation of the calibrated material parameters. Fig. 4 shows the comparison between the experimental results and the model predictions with the identified material parameters summarized in Table 2.

The combination of viscous and pseudo-elastic material behavior captures the material response of the unfilled Elastosil silicone satisfyingly well.

### 3.2. Identification of the mechanical parameters of particle filled silicone

So far the material parameters for the unfilled silicone are identified as described step by step in the previous sections. Now, the parameters taking into account for the influences of the filler particles will be identified. For this, we derive the Piola stress in the stretching direction from Eq. (10), which reads

$$P^{el} = \frac{4}{3}\left[ X_{el} c_1^{el} + 2X_{el}^2 c_2^{el}\left[\lambda^2 + 2\lambda^{-1} - \dim\right] + 3X_{el}^3 c_3^{el}\left[\lambda^2 + 2\lambda^{-1} - \dim\right]^2 \right]\left[\lambda - \lambda^{-2}\right]. \tag{25}$$

with $X_{el} = 1 + g_1^{el} v_f + \left[g_1^{el} v_f\right]^2$

With this, the material parameters $g_1^{el}$ and $g_2^{el}$ are next identified by fitting the analytical solution to the equilibrium curves obtained from the multistep relaxation tests with different filler concentrations. The comparisons between the model predictions and the experimental data are depicted in Figs. 5 to 8 for values $g_1^{el} = 2.81 \cdot 10^{-2}$ and $g_2^{el} = -1.323$.

.

In order to fully characterize the mechanical response of the filled silicone, we will now identify the remaining parameters that were

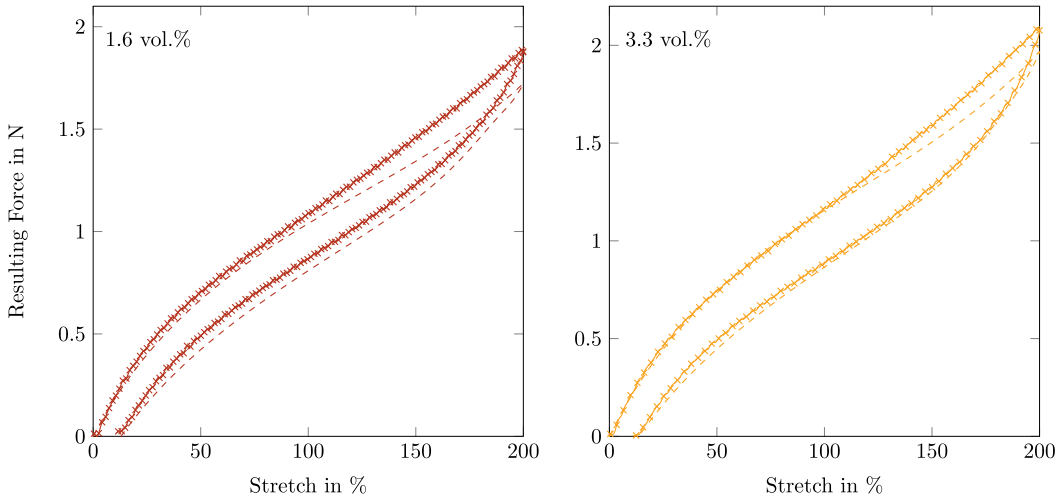


(a) Loading-unloading tests with filler fractions of 1.6 vol.% and 3.3 vol.%

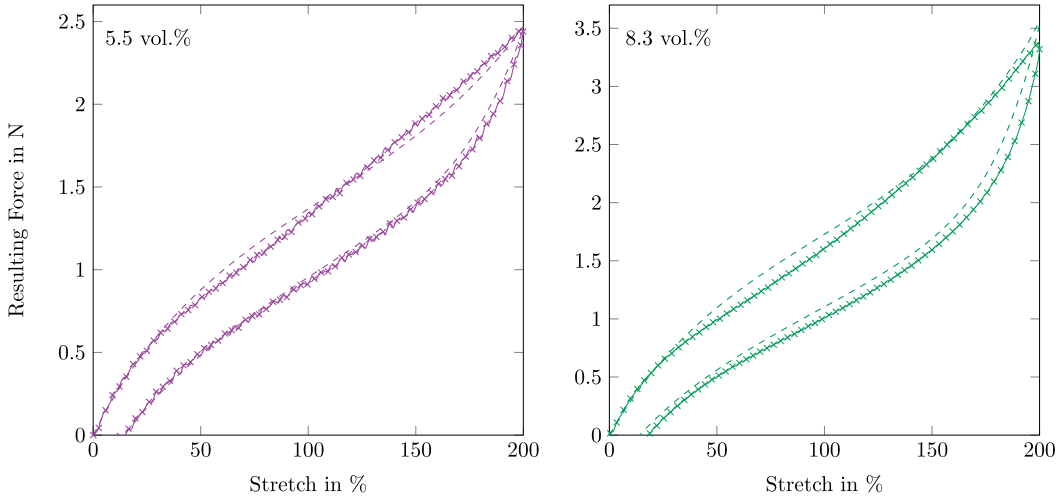


(b) Loading-unloading tests with filler fractions of 5.5 vol.% and 8.3 vol.%

**Fig. 8.** Comparisons between the experimental results (x-marks) and the simulation (dashed lines) of cyclic loading–unloading experiments for Elastosil P 7670™ with various filler contents at a stretch rate of 0.4 $s^{-1}$.

introduced in Eq. (11). To this end, the Neo-Hookean type viscous contributions of the Piola stress in the deformation direction are calculated as

$$\begin{aligned} P_i^v &= \frac{4}{3} X_v \mu_i^v \left[\lambda A_i^2 - \lambda^{-2} A_i^{-1}\right], \\ \dot{A}_i &= \frac{1}{3 X_{\tau,i} \tau_i} \left[\lambda^2 A_i^{-1} - A_i^2 \lambda^{-1}\right] \quad \text{with } i = 1, 2, \\ X_v &= 1 + g_1^v v_f + \left[g_2^v v_f\right]^2, \\ X_{\tau,i} &= 1 + g_{i,1}^\tau v_f + \left[g_{i,2}^\tau v_f\right]^2 \end{aligned} \tag{26}$$

while the Yeoh-type contributions take the form

$$\begin{aligned} P_3^v &= \frac{4}{3} \left[X_v c_1^v + 2 X_v^2 c_2^v \left[\overline{I}_{1,3}^v - 3\right] + 3 X_v^3 c_3^v \left[\overline{I}_{1,3}^v - 3\right]^2\right] \left[\lambda A_3^{-2} - \lambda^{-2} A_3\right], \\ \dot{A}_3 &= \Big[ \frac{1}{3 X_{\tau,3} \tau_{3,1}} + \frac{2}{3 X_{\tau,3} \tau_{3,2}} [\overline{I}_{1,3}^v - \text{dim}] \\ &\quad + \frac{1}{X_{\tau,3} \tau_{3,3}} [\overline{I}_{1,3}^v - \text{dim}]^2 \Big] \left[\lambda^2 A_3^{-1} - A_3^2 \lambda^{-1}\right], \\ \text{with} \quad \overline{I}_{1,3}^v &= \lambda^2 A_3^{-2} + 2\lambda^{-1} A_3, \end{aligned} \tag{27}$$

In combination with the previously derived stress contributions and the identified material parameters, this expression can be fit to multiple data sets of the cyclic loading experiments performed with various filler concentrations. Once again, a *simultaneous minimization* technique is used and the results of the experiments with 8.3 vol.% and 5.5 vol.% fillers at a stretch rate of 0.2 $s^{-1}$ and 0.6 $s^{-1}$ are used as input data for the optimization. This leads to a fit of the analytical solution to the experiments as presented in the Figs. 6 to 9 while the identified material parameters as given in Table 3

**Table 3**
Identified viscous material parameters for filled Elastosil P 7670™.

| $g_1^v$ | $g_2^v$ | $g_{1,1}^\tau$ | $g_{2,1}^\tau$ | $g_{1,2}^\tau$ | $g_{2,2}^\tau$ | $g_{1,3}^\tau$ | $g_{2,3}^\tau$ |
|---|---|---|---|---|---|---|---|
| 4.267 | 0.405 | −4.105 | 6.804 | −4.105 | 6.804 | 6.794 | 1.081 |

### 3.3. Identification of the electro-mechanical coupling parameters of particle filled silicone

The identified mechanical parameters are now used as the basis for the characterization of the electro-mechanical coupling parameters. For electro-mechanical tests, the dimensions of the material samples have to be increased for the application of sufficient amount of electric field. Hence, it is not possible to find an analytical solution to the cyclic tests

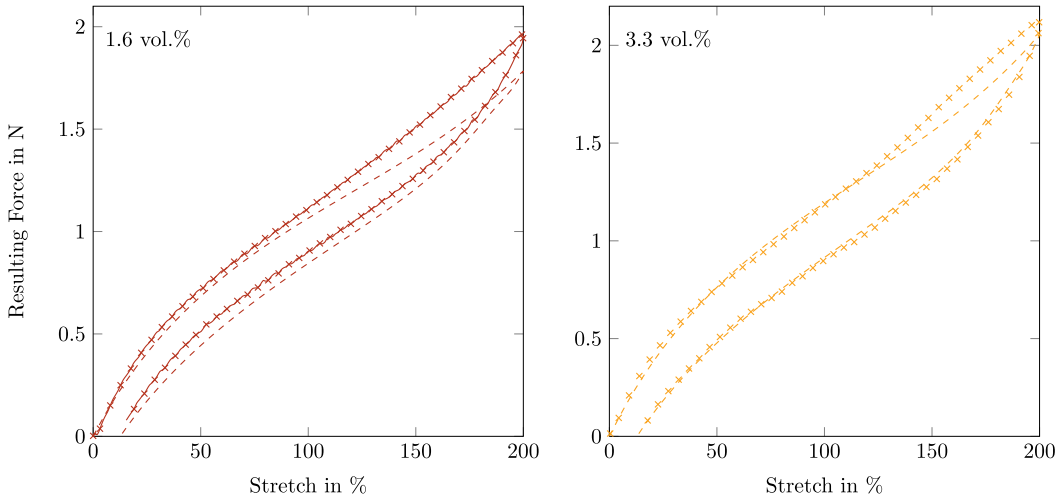


(a) Loading-unloading tests with filler contents of 1.6 vol.% and 3.3 vol.%

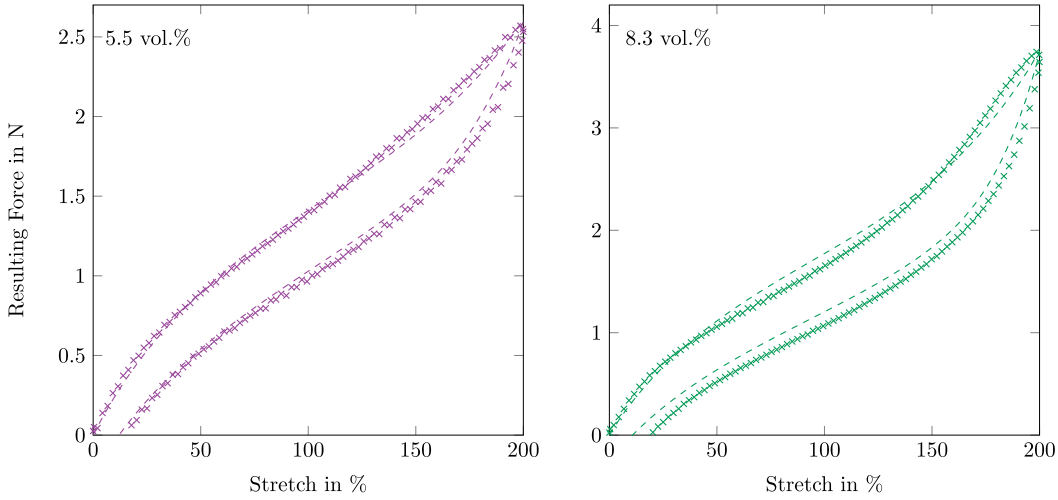


(b) Loading-unloading tests with filler contents of 5.5 vol.% and 8.3 vol.%

**Fig. 9.** Comparisons between the experimental results (x-marks) and the simulation (dashed lines) of cyclic loading–unloading experiments for Elastosil P 7670™ with various filler contents at a stretch rate of 0.6 $s^{-1}$.

under an electro-mechanical load. Thus, the derived material model is implemented into a finite element code (Mehnert et al., 2017, 2018, 2021). This numerical solution is then fitted to the experimental results in order to obtain the electro-mechanical coupling parameters $\gamma$, $\beta^e$ and $k$. The resulting fit is shown in Fig. 10 for the unfilled silicone and Fig. 11 for the particle filled material. The identified parameters are $\gamma = 4.41 \cdot 10^{-14}$, $\beta^e = 4.375 \cdot 10^{-13}$ and $k = 200$.

The Figures show that the material model is capable of simulating the general material response of both pure silicone and the particle filled polymers. It should be emphasized that the response of this non-homogeneous experiment in the case that no electric potential difference is applied, relies solely on the material parameters identified earlier. Due to the increased complexity during the fabrication and the conduction of the experiments the simulation does not fit the experimental results as closely as in the uniaxial case presented in the previous sections. However, the quality of the fit is still satisfying and can therefore be considered as a validation of the purely mechanical material response. Considering the case that an electric field is applied during the experiments, it can be seen that the simulation still replicates the response of the material well. The identified values of the material parameters are summarized in Table 4.

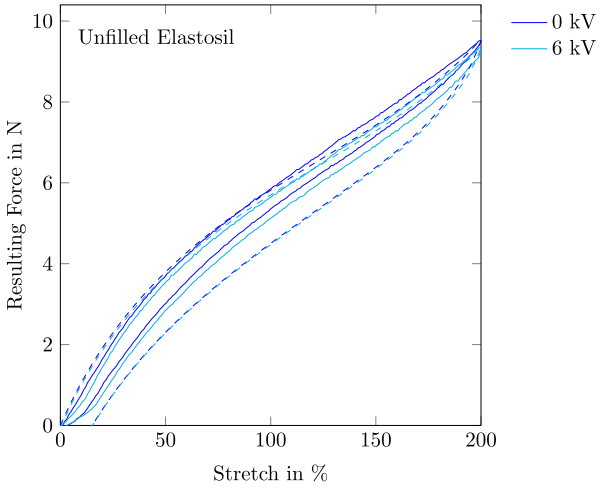


**Fig. 10.** Comparison between the experimental results (solid lines) and the simulation (dashed lines) of cyclic loading–unloading experiments with unfilled Elastosil and a stretch rate of 0.1$s^{-1}$ with an applied electric voltage differences of 0 kV and 6 kV.

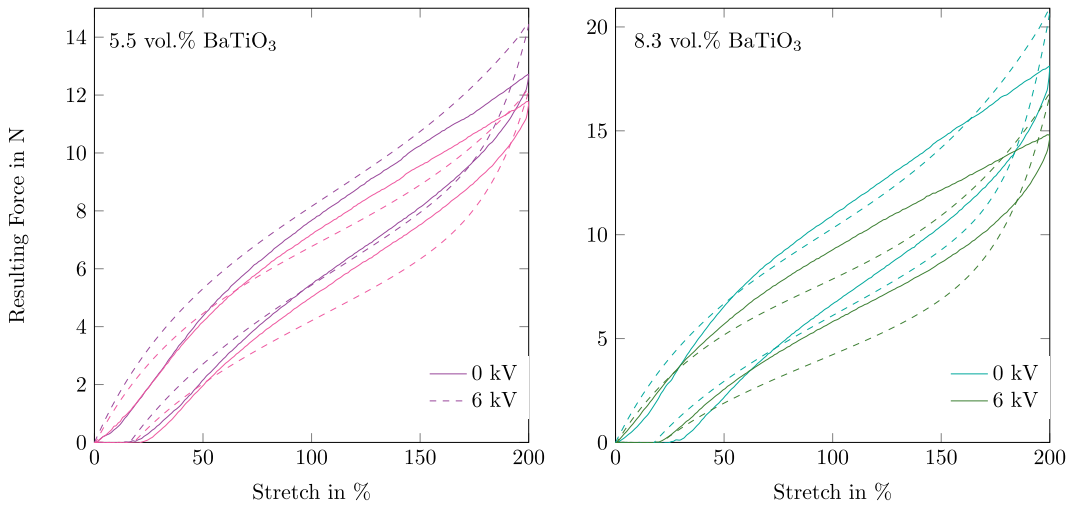


**Fig. 11.** Comparisons between the experimental results (solid lines) and the simulation (dashed lines) with Elastosil filled with (left) 5.5 vol.% $BaTiO_3$ and (right) 8.3 vol.% $BaTiO_3$ at a stretch rate of 0.1 $s^{-1}$ for electric voltage differences of 0 kV and 6 kV.

**Table 4**
Summary of the identified material parameters of the modeling approach for Elastosil P 7670$^{TM}$ filled with $BaTiO_3$ particles. Parameters $c_i$, $\mu_i^v$ in N/mm$^2$, $\tau_i$ in s, $\beta^e$ in N/(Vmm)$^2$, $\gamma$ in N/V$^2$.

| | | | | |
|---|---|---|---|---|
| **Elastosil P 7670$^{TM}$ filled with $BaTiO_3$ particles** | | | | |
| **Mechanical Base Parameters** | | | | |
| Elastic Parameters | | | | |
| $\hat{c}_1^{el}$ | | $c_2^{el}$ | | $c_3^{el}$ |
| 0.0458 | | −0.0012 | | $9.9 \cdot 10^{-5}$ |
| Pseudo-Elastic Parameters | | | | |
| $\hat{\mu}$ | $r$ | $m$ | $a$ | $b$ |
| 0.45 | 1.14 | 0.3427 | 0.42 | 4.564 |
| Viscous Parameters | | | | |
| $\mu_1^v$ | $\mu_2^v$ | $c_1^v$ | $c_2^v$ | $c_3^v$ |
| $4.14 \cdot 10^{-3}$ | $2.57 \cdot 10^{-3}$ | $6.51 \cdot 10^{-3}$ | $2.22 \cdot 10^{-14}$ | $4.04 \cdot 10^{-6}$ |
| $\tau_1$ | $\tau_2$ | | $\tau_3$ | |
| $4.39 \cdot 10^{-3}$ | 0.685 | | 0.266 | |
| **Particle Scaling Parameters** | | | | |
| Elastic Scaling Parameters | | | | |
| $g_1^{el}$ | | $g_2^{el}$ | | |
| $2.81 \cdot 10^{-2}$ | | −1.323 | | |
| Viscous Scaling Parameters | | | | |
| $g_1^v$ | $g_2^v$ | $g_{1,1}^\tau$ | $g_{2,1}^\tau$ | $g_{1,2}^\tau$ | $g_{2,2}^\tau$ | $g_{1,3}^\tau$ | $g_{2,3}^\tau$ |
| 4.267 | 0.405 | −4.105 | 6.804 | −4.105 | 6.804 | 6.794 | 1.081 |
| **Electro-Mechanical Coupling Parameters** | | | | |
| $\beta^e$ | | $\gamma$ | | $k$ |
| $4.375 \cdot 10^{-13}$ | | $4.41 \cdot 10^{-14}$ | | 200 |

## 4. Deformation of a cylinder under thermo-electric loading

As a simple yet illustrative numerical example, we present the deformation of a cylinder that is fixed in normal direction on one of its plane faces and loaded by an electric potential difference between the fixed and the opposing face, which results in a homogeneous deformation of the geometry. The purpose of this numerical investigation is to present the effects of the electric field on the mechanical response of the viscous material. In contrast to the experiments presented in the preceding sections where the material response was dominated by the imposed mechanical deformation, the deformation of the cylinder is directly induced by the application of an electric field. These calculations are performed using the presented material model and the material parameters identified in the previous sections. In order to link this example to the experiments, the height of the investigated cylinder is 0.3 mm, as an approximation of the thickness of a material sample of Elastosil at the maximum deformation of 200%. Furthermore, the potential difference applied between the plane faces of the cylinder is prescribed as 6 kV, which is the maximum potential difference applied in the experimental investigations. The potential difference is linearly increased over a specific ramp-up time $t^{\text{ramp}}$ and is reduced back to zero over the same time to illustrate the viscous response of the material. The results are computed using the finite element implementation of the presented modeling approach.We assume that the geometry and the boundary conditions of the example are symmetric in relation to the center axis of the cylinder and the resulting deformation does not lead to a displacement of the material perpendicular to the cross section. Thus, the finite element model can be reduced to a quarter of the cross section of the cylinder in form of a two-dimensional mesh. This cross-section is a square with a side length of 0.15 mm and is discretized with 64 four-node elements. A sketch of the geometry with the prescribed boundary conditions and a plot of the simulated cross section of the cylinder in the deformed state is presented in Fig. 12. It should be noted that as the resulting deformation is comparatively small, the result presented in the right plot is scaled by a factor of 2 and the initial geometry of the cylinder is depicted with reduced opacity for the sake of visibility. Now, a periodic loading of the cylinder is assumed such that in each cycle the magnitude of the electric potential difference is increased to the maximum value and then decreased to zero. The resulting normal displacement of the center of the top surface of the cylinder is depicted in Fig. 13 for five cycles and various loading conditions.

The response of the cylinder illustrates both the effects of the addition of particles and the characteristics of the selected material model. Initially we will focus on the response of the unfilled silicone presented in the left plot of Fig. 13. It can be seen that the cylinder does not return to its initial configuration after the first cycle due to the viscous stress contributions. However, in the following cycles the cylinder returns almost exactly to the state at the beginning of the respective cycle, showing that the viscous characteristics of the unfilled material influence the overall response only slightly. This is emphasized even further by the fact that the ramp-up time has only a meager effect on the maximum displacement of the cylinder. When compared to the displacement of the filled material as shown in the right plot of Fig. 13, it is clearly visible that the addition of particles with a high dielectric constant leads to a distinctly more pronounced displacement. As before, the cylinder does not return to its initial configuration after the end of

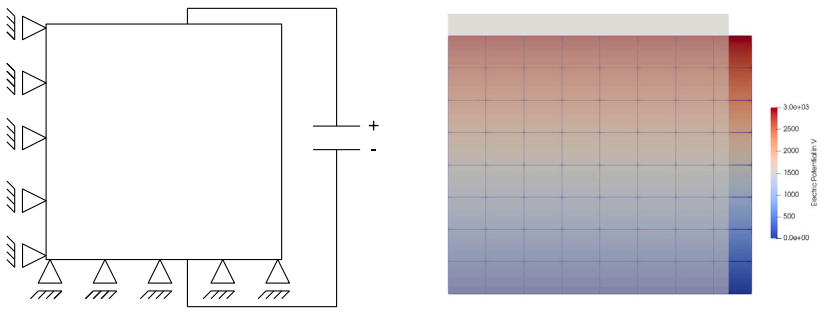


**Fig. 12.** (left) A sketch of the model geometry with prescribed boundary conditions. (right) Resulting deformation of the cross section under thermo-electric loading for a ramp-up time of $10^3$ s at reference temperature, deformation scaled by a factor of 2.

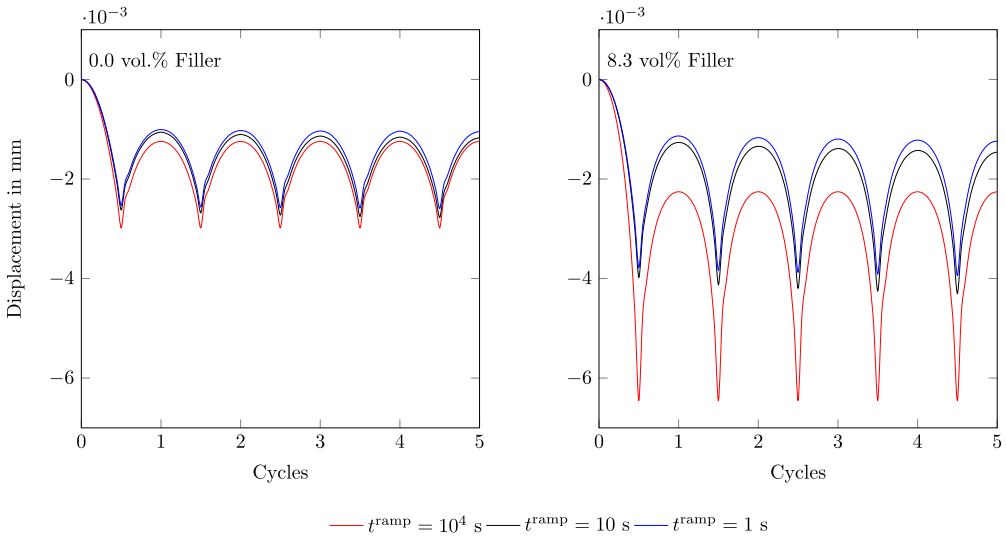


**Fig. 13.** Displacement of the center of the top surface of a cylinder of (left) pure Elastosil and (right) Elastosil filled with 8.3 vol.% $BaTiO_3$ particles for different ramp-up times of the electric field.

the first cycle due to the viscous stress. However, now it can be seen that the viscous characteristics of the compound have a very distinct influence on the material response. First, the response is much more pronounced when the electric field is increased over a longer period of time as the elastic contributions are dominating the response. When the ramp-up time is reduced on the other hand, the displacement is reduced significantly as the viscous contributions start to dominate the material response. Second, a close analysis of the displacement of the cylinder at the end of each cycle shows that this deformation increases with each cycle adding a viscous contribution to the deformation.

Taken together, for the application of this type of silicone, it is crucial to consider the desired rate of deformation. Even though the addition of $BaTiO_3$ particles leads to an increase of the effect of the electric field on the material, the resulting deformation is markedly dominated by the deformation rate and can drastically impact the realized deformation.

## 5. Conclusion and outlook

In this contribution, a numerical modeling approach for the simulation of particle filled dielectric elastomers under combined electro-mechanical loading was presented. The proposed model was specified for the viscoelastic silicone Elastosil P 7670$^{TM}$ filled with Barium-Titanate particles. In combination with the experimental results presented in Part I of this sequel, all relevant material parameters appearing in the constitutive model were identified here. For the replication of the mechanical experiments, analytical solutions were derived whereas in the case of an electro-mechanical load, the solution was calculated using an electro-mechanically coupled finite-element implementation.In our future work, we plan to combine the approach proposed herein with homogenization techniques in order to reduce the number of fitting parameters and analyze the interactions between the silicone and the filler particles in more detail similar to the recent studies shown in Ghosh et al. (2021).

## CRediT authorship contribution statement

**Markus Mehnert:** Conceptualization, Methodology, Software, Validation, Investigation, Data curation, Writing – original draft, Visualization. **Jessica Faber:** Investigation, Data curation, Writing – original draft, Visualization. **Mokarram Hossain:** Conceptualization, Methodology, Writing – review & editing. **Shawn A. Chester:** Writing – review & editing, Supervision. **Paul Steinmann:** Writing – review & editing, Supervision, Funding acquisition.

## Declaration of competing interest

The authors declare that they have no known competing financial interests or personal relationships that could have appeared to influence the work reported in this paper.

## Acknowledgments

M. Mehnert and P. Steinmann acknowledge the funding within the DFG, Germany project No. STE 544/52-2 and GRK2495/C. M. Hossain would like to extend his sincere appreciation to Engineering

and Physical Sciences Research Council (EPSRC), United Kingdom for an Impact Acceleration Award (EP/R511614/1). The financial support by the Deutsche Forschungsgemeinschaft (DFG, German Research Foundation) Projekt nummer 326998133 - TRR 225 (subproject B09) to J. Faber is gratefully acknowledged. S. Chester acknowledges partial support from the US National Science Foundation under grant number CMMI-1751520.

## References

Amin, A., Alam, M., Okui, Y., 2002. An improved hyperelasticity relation in modeling viscoelasticity response of natural and high damping rubbers in compression: Experiments, parameter identification and numerical verification. Mech. Mater. 34 (2), 75–95.

Ask, A., Menzel, A., Ristinmaa, M., 2012. Electrostriction in electro-viscoelastic polymers. Mech. Mater. 50, 9–21.

Bar-Cohen, Y., 2002. Electroactive polymers: Current capabilities and challenges. In: SPIE's 9th Annual International Symposium on Smart Structures and Materials. International Society for Optics and Photonics, pp. 1–7.

Bar-Cohen, Y., 2004. Electroactive Polymer (EAP) Actuators As Artificial Muscles: Reality, Potential, and Challenges, Vol. 136. SPIE Press.

Bergstrom, J.S., Boyce, M.C., 1999. Mechanical behavior of particle filled elastomers. Rubber Chem. Technol. 72 (4), 633–656.

Böse, H., Fuß, E., 2014. Novel dielectric elastomer sensors for compression load detection. In: SPIE Smart Structures and Materials+ Nondestructive Evaluation and Health Monitoring. International Society for Optics and Photonics, p. 905614.

Carpi, F., 2010. Electromechanically active polymers. Polym. Int. 59 (3), 277–278.

Collins, I., Hossain, M., Dietmer, W., Masters, I., 2021. Flexible membrane structures for wave energy harvesting: A review of the developments, materials and computational modelling approaches. Renew. Sustain. Energy Rev. 151, 111478.

Dorfmann, A., Ogden, R.W., 2004. A constitutive model for the mullins effect with permanent set in particle-reinforced rubber. Int. J. Solids Struct. 41 (7), 1855–1878.

Dorfmann, A., Ogden, R., 2005. Nonlinear electroelasticity. Acta Mech. 174 (3–4), 167–183.

Dorfmann, A., Ogden, R., 2006. Nonlinear electroelastic deformations. J. Elasticity 82 (2), 99–127.

Ericksen, J., 2007. Theory of elastic dielectrics revisited. Arch. Ration. Mech. Anal. 183 (2).

Eringen, A.C., 1963. On the foundations of electroelastostatics. Internat. J. Engrg. Sci. 1 (1), 127–153.

Francfort, G.A., Gloria, A., Lopez-Pamies, O., 2021. Enhancement of elasto-dielectrics by homogenization of active charges. J. Math. Pures Et Appl. 156, 392–419.

Fung, Y., Fronek, K., Patitucci, P., 1979. Pseudoelasticity of arteries and the choice of its mathematical expression. Am. J. Physiol.-Heart Circulat. Physiol. 237 (5), H620–H631.

Ghosh, K., Guo, J., Lopez-Pamies, O., 2019. Homogenization of time-dependent dielectric composites containing space charges, with applications to polymer nanoparticulate composites. Int. J. Non-Linear Mech. 116, 155–166.

Ghosh, K., Shrimali, B., Kumar, A., Lopez-Pamies, O., 2021. The nonlinear viscoelastic response of suspensions of rigid inclusions in rubber: I—Gaussian rubber with constant viscosity. J. Mech. Phys. Solids 154, 104544.

Guth, E., 1945. Theory of filler reinforcement. J. Appl. Phys. 16 (20), 20–25.

Holzapfel, G.A., Simo, J.C., 1996. A new viscoelastic constitutive model for continuous media at finite thermomechanical changes. Int. J. Solids Struct. 33 (20–22), 3019–3034.

Hossain, M., Steinmann, P., 2013. More hyperelastic models for rubber-like materials: Consistent tangent operators and comparative study. J. Mech. Behav. Mater. 22 (1–2), 27–50.

Hossain, M., Vu, D.K., Steinmann, P., 2012. Experimental study and numerical modelling of VHB 4910 polymer. Comput. Mater. Sci. 59, 65–74.

Huang, C., Zhang, Q., Li, J.Y., Rabeony, M., 2005. Colossal dielectric and electromechanical responses in self-assembled polymeric nanocomposites. Appl. Phys. Lett. 87 (18), 182901.

Kaliske, M., Rothert, H., 1997. Formulation and implementation of three-dimensional viscoelasticity at small and finite strains. Comput. Mech. 19 (3), 228–239.

Keip, M.-A., Steinmann, P., Schröder, J., 2014. Two-scale computational homogenization of electro-elasticity at finite strains. Comput. Methods Appl. Mech. Engrg. 278, 62–79.

Koh, S.J.A., Keplinger, C., Li, T., Bauer, S., Suo, Z., 2011. Dielectric elastomer generators: How much energy can be converted? IEEE/ASME Trans. Mechatronics 16 (1), 33–41.

Koprowski-Theiss, N., Johlitz, M., Diebels, S., 2011. Characterizing the time dependence of filled EPDM. Rubber Chem. Technol. 84 (2), 147–165.

Kovetz, A., 2000. Electromagnetic Theory. Oxford University Press Oxford.

Lefevre, V., Lopez-Pamies, O., 2017. Homogenization of elastic dielectric composites with rapidly oscillating passive and active source terms. SIAM J. Appl. Math. 77 (6), 1962–1988.

Lefèvre, V., Lopez-Pamies, O., 2017a. Nonlinear electroelastic deformations of dielectric elastomer composites: I—Ideal elastic dielectrics. J. Mech. Phys. Solids 99, 409–437.

Lefèvre, V., Lopez-Pamies, O., 2017b. Nonlinear electroelastic deformations of dielectric elastomer composites: II—Non-Gaussian elastic dielectrics. J. Mech. Phys. Solids 99, 438–470.

Linder, C., Tkachuk, M., Miehe, C., 2011. A micromechanically motivated diffusion-based transient network model and its incorporation into finite rubber viscoelasticity. J. Mech. Phys. Solids 59 (10), 2134–2156.

Lopez-Pamies, O., 2014. Elastic dielectric composites: Theory and application to particle-filled ideal dielectrics. J. Mech. Phys. Solids 64, 61–82.

Mehnert, M., Hossain, M., Steinmann, P., 2016. On nonlinear thermo-electro-elasticity. Proc. R. Soc. A 472 (2190), 20160170.

Mehnert, M., Hossain, M., Steinmann, P., 2018. Numerical modeling of thermo-electro-viscoelasticity with field-dependent material parameters. Int. J. Non-Linear Mech. 106, 13–24.

Mehnert, M., Hossain, M., Steinmann, P., 2021. A complete thermo-electro-viscoelastic characterization of dielectric elastomers-Part II: Continuum modelling approach. J. Mech. Phys. Solids 157, 104625.

Mehnert, M., Pelteret, J.-P., Steinmann, P., 2017. Numerical modelling of nonlinear thermo-electro-elasticity. Math. Mech. Solids 22 (11), 2196–2213.

Ogden, R.W., 2003. Nonlinear elasticity, anisotropy, material stability and residual stresses in soft tissue. In: Biomechanics of Soft Tissue in Cardiovascular Systems. Springer, pp. 65–108.

Ogden, R.W., Roxburgh, D.G., 1999. A pseudo–elastic model for the Mullins effect in filled rubber. Proc. R. Soc. Lond. Ser. A Math. Phys. Eng. Sci. 455 (1988), 2861–2877.

O'Halloran, A., O'Malley, F., McHugh, P., 2008. A review on dielectric elastomer actuators, technology, applications, and challenges. J. Appl. Phys. 104 (7), 9.

Schröder, J., Keip, M.-A., 2012. Two-scale homogenization of electromechanically coupled boundary value problems. Comput. Mech. 50 (2), 229–244.

Steinmann, P., 2011. Computational nonlinear electro-elasticity - Getting started -. In: Mechanics and Electrodynamics of Magneto-and Electro-Elastic Materials. Springer, pp. 181–230.

Toupin, R.A., 1956. The elastic dielectric. J. Ration. Mech. Anal. 5 (6), 849–915.

Vertechy, R., Fontana, M., Papini, G.R., Forehand, D., 2014. In-tank tests of a dielectric elastomer generator for wave energy harvesting. In: SPIE Smart Structures and Materials+ Nondestructive Evaluation and Health Monitoring. International Society for Optics and Photonics, p. 90561G.

Wang, S., Chester, S.A., 2018. Experimental characterization and continuum modeling of inelasticity in filled rubber-like materials. Int. J. Solids Struct. 136, 125–136.

Zeng, Q., Yu, A., Lu, G., 2008. Multiscale modeling and simulation of polymer nanocomposites. Prog. Polym. Sci. 33 (2), 191–269.